Interpretation of Ir L-edge isotropic x-ray absorption spectra across the pressure-induced dimerization transition in hyperhoneycomb β-Li_2IrO_3

Michel van Veenendaal [1,2] and Daniel Haskel [2]
[1]*Department of Physics, Northern Illinois University, DeKalb, Illinois 60115, USA*
[2]*Advanced Photon Source, Argonne National Laboratory, Argonne, Illinois 60439, USA*

(Received 28 April 2022; revised 6 June 2022; accepted 7 June 2022; published 16 June 2022)

The extended nature of atomic $5d$ orbitals, together with a relatively short $\sim$3 Å Ir-Ir distance across edge-shared octahedra in honeycomb iridate lattices, leads to a tendency to disrupt the local, spin-orbit-entangled $j_{\rm eff} = \frac{1}{2}$ moments of Ir^{4+} ions in favor of dimerization and the formation of molecular orbitals, especially upon lattice compression. The sensitivity of Ir L-edge spectroscopy to both spin-orbit entanglement in $j_{\rm eff}$ states and the quenching of orbital degrees of freedom in dimerized states results in a peculiar evolution of x-ray absorption spectra across dimerization transitions, including energy shifts in the opposite direction for L_3 and L_2 leading absorption edges and substantial changes in their isotropic branching ratio. We present a theoretical description of the evolution of $5d$ electronic states, and related x-ray absorption spectra, in going from the single ion to the dimerized limit. The calculations reproduce the experimental results for hyper-honeycomb β-Li_2IrO_3 [L. Veiga *et al.*, Phys. Rev. B **100**, 064104 (2019); **96**, 140402(R) (2017)] and shed light into the weakening of the coupling between spin and orbital degrees of freedom as the strength of dimerization increases. The results provide a basis for the interpretation of L-edge x-ray absorption spectra in $5d$ systems where competition between the formation of local $j_{\rm eff}$ states and molecular orbitals is at play.

DOI: 10.1103/PhysRevB.105.214420

I. INTRODUCTION

Among various routes being pursued to realize Kitaev's elusive quantum spin liquid state in honeycomb lattices [1], the application of hydrostatic pressure has been widely explored as it allows for continuous tuning of interatomic distances and bond angles regulating the strength and nature of exchange interactions [2–9]. The unique bond-directional exchange anisotropy in Kitaev's model, $K_{ij}^{\gamma} S_i^{\gamma} S_j^{\gamma}$, where K is the Kitaev exchange constant and $\gamma = (X, Y, Z)$ are the three types of NN bonds in the honeycomb lattice, and related frustration inherent to Kitaev's spin liquid state, requires ideal honeycomb structures which are rarely realized in as-grown crystals. Iridate two-dimensional (2D) honeycomb and three-dimensional (3D) hyper/stripy-honeycomb lattices composed of edge-shared IrO_6 octahedra with Ir^{4+} ions are an ideal starting point for the exploration of spin liquid states since the $j_{\rm eff} = \frac{1}{2}$ state of half-filled ($5d^5$) Ir orbitals stabilized by a strong spin-orbit interaction, together with 90° Ir-O-Ir bonding, embody the basic requirements for the emergence of the bond-directional exchange interaction of Kitaev's model [10]. Deviations from the perfect honeycomb lattice introduce competing isotropic Heisenberg $J_{ij}^{\gamma} \mathbf{S}_i^{\gamma} \cdot \mathbf{S}_j^{\gamma}$ and symmetric anisotropic off-diagonal $\Gamma^{\gamma}(S_i^{\alpha} S_j^{\beta} + S_i^{\beta} S_j^{\alpha})$ ($\alpha \neq \beta \neq \gamma$) exchange interactions, which, in addition to possible direct exchange terms, prevent the emergence of Kitaev's spin liquid state, leading instead to magnetically ordered ground states. Both zig-zag and incommensurate counterrotating magnetic order was observed in 2D-α and 3D-(β, γ) harmonic honeycomb [11] structures of Na_2IrO_3 and Li_2IrO_3 [12–15] at ambient pressure, with $KJ\Gamma$ microscopic spin Hamiltonians providing a theoretical framework [16–18].

Here we focus on polymorphs of Li_2IrO_3 whose electronic and magnetic ground states undergo dramatic changes under compression. In particular, the $\beta(\gamma)$ hyper(stripy)-honeycomb phases loose magnetic order at a first-order transition around 1.5 GPa, which is clearly seen in x-ray magnetic circular dichroism [3,19], x-ray magnetic scattering [8], muon spin resonance [20], and magnetometry [7] measurements. While local pseudospin $j_{\rm eff} = \frac{1}{2}$ moments required to map the exchange interactions in honeycomb structures with edge-shared octahedra into the bond-directional exchange of Kitaev's model [10] are present at ambient pressure [19], both x-ray absorption spectroscopy [2,3] and resonant inelastic x-ray scattering [6] measurements show that the pressure-induced loss of magnetic order is accompanied by a reconstruction of $5d$ electronic states as evidenced in a strong suppression of Ir $L_{2,3}$ isotropic branching ratio [2,3] and disappearance of $j_{\rm eff} = \frac{3}{2} \rightarrow \frac{1}{2}$ excitation [6]. Low-temperature x-ray diffraction measurements revealed that a pressure-induced dimerization transition takes place in the same pressure range as the electronic reconstruction, whereby Ir ions in one of the (X, Y, Z) bonds of the honeycomb lattice form dimers with strongly reduced interatomic distances in the 2.6–2.7 Å range, comparable to the interatomic distance in Ir metal [2].

The nature of the electronic states in the dimerized phase of β-Li_2IrO_3, and in particular how the electronic states evolve from a $j_{\rm eff}$ description to a description in terms of molecular orbitals, has not been fully addressed. Density functional theory provides some insight into the possible nature of

dimerized states [6], but a clear connection to experimental signatures has not been presented. A very peculiar signature is indeed observed in the isotropic x-ray absorption spectra of Ir $L_{2,3}$ edges across the dimerization transition: the leading absorption edge at L_3 and L_2 resonances shift in opposite directions as the electronic reconstruction takes place [2]. A more typical behavior would be for both edges to shift in the same direction, for example, as a result of pressure-induced charge transfer and the related change in the oxidation state. Clearly the disparate response of the transitions at spin-orbit split $2p_{\frac{1}{2},\frac{3}{2}}$ core levels is related to the relevance of spin-orbit interactions in the $5d$ states probed by electric dipole transitions since their $j = \frac{3}{2}, \frac{5}{2}$ character (or absence thereof) dictates which of the empty $5d$ valence states are accessible from these two core levels. In what follows we present a theoretical derivation of the isotropic x-ray absorption spectra at Ir $L_{2,3}$ edges based on configuration interaction calculations [21] with variable strength of dimerization between Ir ions. The results provide a quantitative description of how the evolution from the j_{eff} ionic limit to dimerized orbitals causes a shift of leading $L_{2,3}$ absorption edges in opposite directions and reduces the expectation value of the spin-orbit interaction in $5d$ states, in close agreement with the experiment [2,3].

II. THEORY

Due to the large lifetime broadening of the Ir $2p$ core level, the absorption spectra can often be rather well described within the atomic limit, as long as the character of the local moment is well captured [22,23]. However, since the dimerization affects the effective moment, the x-ray absorption spectroscopy (XAS) spectra for Li_2IrO_3 are described using a dimer. For each atom in the dimer, a local octahedral field splits the $5d$ orbitals into t_{2g} and e_g irreducible representations. The size of the octahedral field [24] is taken as $10Dq = 3.2$ eV. The spin-orbit interaction $\zeta \mathbf{L} \cdot \mathbf{S}$ is sizable and taken as $\zeta = 0.3$ eV [22]. This splits the t_{2g} orbitals into effective spin-orbit levels with $j_{\text{eff}} = \frac{3}{2}, \frac{1}{2}$ [10,25]. To include the effects of dimerization, we take a two-site model. Since the coupling between different iridium atoms is across edge-shared octahedra, one of the real t_{2g} couples most strongly with the neighboring orbital of the same type [26]. The hopping matrix element is $-V$ with $V > 0$ and is varied to observe the trends. Since we are only interested in the isotropic spectrum, the results are the same regardless of whether the coupling is between the xy, yz, or zx orbital.

Figure 1 shows the results for the x-ray absorption at the Ir L edge. To simulate the increased dimerization due to pressure, the hopping matrix element V is varied from 0 to 1.6 eV. Before going into more detail, we note that the experimental trends [2,3] are reproduced. The leading edge of the L_3 edge moves to higher energy with increasing pressure. At the same, time the L_2 edge moves in the opposite direction. Additionally, the branching ratio, i.e., the ratio I_{L_3}/I_{L_2} of the integrated absorption intensities at the L_3 and L_2 edges, decreases. These changes are primarily caused by changes into the lowest unoccupied states. The excitations into the e_g orbitals are relatively unaffected by the dimerization. The changes occur primarily at the leading edge of the absorption edges, which are mainly due to excitations into empty t_{2g}-derived states, shown separately in Fig. 1. There are two effects that change the spectral line shape. First, the antibonding t_{2g} states move to higher energy. This explains the shift to the higher energy of the L_3 edge. The shift also occurs at the L_2 edge. However, it does not lead to an apparent shift to higher energy of the L_2. This is because the intensity of the t_{2g} spectral weight increases when the dimerization increases. Due to the decreased $j_{\text{eff}} = \frac{1}{2}$ character, the antibonding t_{2g} states become accessible at the L_2 edge ($2p_{\frac{1}{2}}$ core level excitation). This effectively shifts the weight of the entire edge to the lower energy.

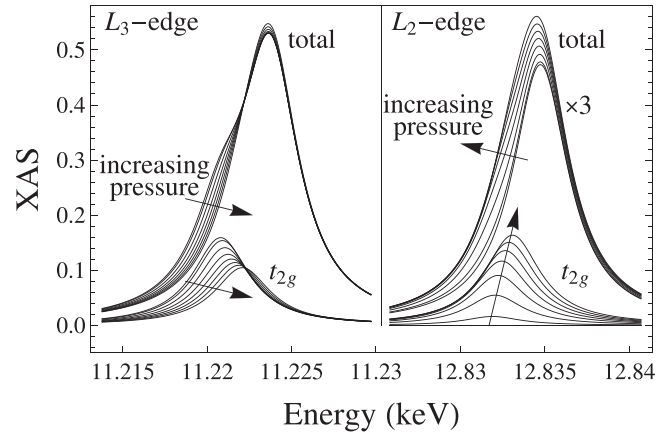

FIG. 1. The x-ray absorption at the iridium L edges as a function of pressure. The pressure is simulated by increasing the coupling between the two iridium ions in the calculation increasing the strength of the dimerization. The hopping matrix element V varies from 0 to 1.6 eV in eight steps. Both the total absorption spectra and the partial absorption into the low-energy states (labeled as t_{2g} for simplicity) are shown.

Let us look at the trends more closely. The standard approach [10] is to consider the t_{2g} orbitals as an effective p orbital

$$
\begin{aligned}
|1_{\text{eff}}\rangle &= |-1\rangle = \frac{1}{\sqrt{2}}(|zx\rangle - i|yz\rangle), \\
|0_{\text{eff}}\rangle &= \frac{1}{\sqrt{2}}(|2\rangle - |-2\rangle) = i|xy\rangle, \\
|-1_{\text{eff}}\rangle &= -|1\rangle = \frac{1}{\sqrt{2}}(|zx\rangle + i|yz\rangle),
\end{aligned} \tag{1}
$$

where $|m_{\text{eff}}\rangle$ with $m_{\text{eff}} = 1, 0, -1$ are the effective atomic p orbitals, $|m\rangle$ with $m = 2, 1, 0, -1, -2$ are the atomic d orbitals, and $|\mu\rangle$ with $\mu = xy, yz, zx$ are the t_{2g} orbitals. The phases are chosen such that the spin-orbit interaction for the effective p orbital is equivalent to that of a p orbital for an atom. Note that $m_{\text{eff}} = -m$ only for $m_{\text{eff}} = \pm 1$. This is because the $m_{\text{eff}} = 0$ component is not the $m = 0$ (the $3z^2 - r^2$ orbital), but the xy orbital, which is a combination of the $m = \pm 2$ atomic orbitals.

In the absence of dimerization, the spin-orbit interaction splits the t_{2g} orbitals into $j_{\text{eff}} = \frac{3}{2}, \frac{1}{2}$ states. The low-energy physics is determined by the $j_{\text{eff}} = \frac{1}{2}$ states which are half filled and can be expressed as

$$
\left|\frac{1}{2}, \pm\frac{1}{2}\right\rangle = \sqrt{\frac{2}{3}}\left|1_{\text{eff}}, \mp\frac{1}{2}\right\rangle - \frac{1}{\sqrt{3}}\left|0_{\text{eff}}, \pm\frac{1}{2}\right\rangle, \tag{2}
$$

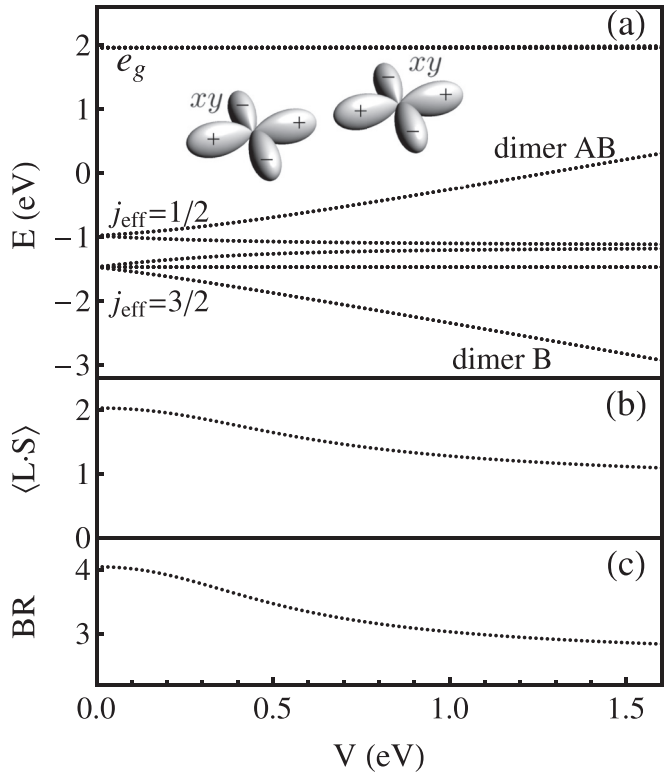

FIG. 2. (a) The energies of the different levels in the iridium dimer as a function of the hopping matrix element V. The $j_{\rm eff}$ states correspond to the $V = 0$ case. Upon increasing the hopping matrix element V, these states split. For larger V, two clear dimer states are formed corresponding to the bonding (B) and antibonding (AB) states. (b) The ground-state expectation value $\langle \mathbf{L} \cdot \mathbf{S} \rangle$ of the spin-orbit coupling. (c) The branching ratio I_{L_3}/I_{L_2}.

where the spin componentis added to the wave functions. The $|\frac{3}{2}, \pm\frac{1}{2}\rangle$ states are orthogonal to $|\frac{1}{2}, \pm\frac{1}{2}\rangle$. The other components are $|\frac{3}{2}, \pm\frac{3}{2}\rangle = |\pm 1_{\rm eff}, \pm\frac{1}{2}\rangle$. The spin-orbit coupling can be obtained $\langle \mathbf{l} \cdot \mathbf{s} \rangle = -\langle \mathbf{l}_{\rm eff} \cdot \mathbf{s} \rangle = -\frac{1}{2}[j_{\rm eff}(j_{\rm eff}+1) - l_{\rm eff}(l_{\rm eff}+1) - s(s+1)] = -\frac{1}{2}[j_{\rm eff}(j_{\rm eff}+1) - \frac{11}{4}]$ with $s = \frac{1}{2}$, where $\langle \mathbf{l} \cdot \mathbf{s} \rangle$ indicates the spin-orbit coupling for a single state (not to be confused with $\langle \mathbf{L} \cdot \mathbf{S} \rangle$, which is the ground-state expectation value of the spin-orbit coupling of the many-electron state). This gives $\langle \mathbf{l} \cdot \mathbf{s} \rangle = -\frac{1}{2}, 1$ for $j_{\rm eff} = \frac{3}{2}, \frac{1}{2}$, respectively. Note that for the x-ray absorption sum rules, the spin-orbit coupling for the d orbitals is relevant, which is opposite to that of the effective p orbitals.

Since the spin-orbit coupling is $\langle \mathbf{l} \cdot \mathbf{s} \rangle = -\frac{1}{2}, 1$ for $j_{\rm eff} = \frac{3}{2}, \frac{1}{2}$, respectively, the local energies in the absence of dimerization are $-4Dq - \frac{1}{2}\zeta$, $-4Dq + \zeta$, and $6Dq$ for $j_{\rm eff} = \frac{3}{2}, \frac{1}{2}$, and the e_g orbitals, respectively, see Fig. 2(a). The results at ambient pressure are comparable to $V \cong 0$ [6]. An Ir^{4+} ion has five electrons in the $5d$ orbital, which means the $j_{\rm eff} = \frac{3}{2}$ is fully occupied and the $j_{\rm eff} = \frac{1}{2}$ state is half filled.

The dimerization couples a pair of real t_{2g} orbitals on neighboring sites. The IrO_6 octahedra are edge sharing, implying that the same type of orbitals couple to each other. Let us take the dimerization along the (110) direction, so that two xy orbitals are coupled. In the absence of spin-orbit coupling, this interaction is given by

$$H_{\rm dimer} = \begin{pmatrix} 0 & -V \\ -V & 0 \end{pmatrix}, \tag{3}$$

where the basis is $|xy_i\sigma\rangle$ where $\sigma = \pm\frac{1}{2}$ is the spin and the subscript in xy_i with $i = 1, 2$ labels the different sites in the dimer. We take $V > 0$, meaning the lobes of the orbitals along the dimerization direction have the same sign. Dimerization of the xy orbital, which corresponds to the $m_{\rm eff} = 0$ component, is convenient with the choice of our axis system for the orbitals in Eq. (1). Note that dimerization along any other direction corresponds to a reorientation of the coordinate system and the end results are the same. When only looking at the dimerization, the solutions are given by bonding (B) and antibonding (AB) states of the xy orbitals

$$|{\rm B/AB}, \sigma\rangle = \frac{1}{\sqrt{2}}(|xy_1\sigma\rangle \pm |xy_2\sigma\rangle) \tag{4}$$

$$= -\frac{i}{\sqrt{2}}(|0_{{\rm eff},1}\sigma\rangle \pm |0_{{\rm eff},2}\sigma\rangle). \tag{5}$$

A comparison with Eqs. (1) and (2) shows that the dimerization competes with the formation of local $j_{\rm eff}$ moments. The dimerization would like to make states of pure xy or $0_{\rm eff}$ character; the spin-orbit interaction prefers to mix these orbitals with $1_{\rm eff}$ states of opposite spin. Therefore the dimerization mixes the $j_{\rm eff} = \frac{3}{2}$ and $j_{\rm eff} = \frac{1}{2}$ states.

As we can see in Fig. 2(a), the dimerization causes the bonding and antibonding states to split off from the other t_{2g} states. Although it appears that the bonding and antibonding states arise from the $j_{\rm eff} = \frac{3}{2}$ and $\frac{1}{2}$, respectively, the mixing between the $j_{\rm eff}$ states progressively increases for larger values of V. High-pressure band-structure calculations give the splitting $2V$ between the bonding and antibonding states of the order of 2.4 eV [6]. This corresponds to $V \cong 1.2$ eV. Since the antibonding dimer is unoccupied, it is visible in the absorption spectrum. The decrease in energy between the antibonding dimer and the e_g levels (which form the main line in the spectrum) as V or pressure increases is clearly observed at the L_3 edge.

Figures 2(b) and 2(c) give the trends for the expectation value $\langle \mathbf{L} \cdot \mathbf{S} \rangle$ of the spin-orbit coupling and the branching ratio. The branching ratio BR of the isotropic x-ray absorption spectrum is intimately related to $\langle \mathbf{L} \cdot \mathbf{S} \rangle$ [22,27] with ${\rm BR} = (2+r)/(1-r)$ where $r = \langle \mathbf{L} \cdot \mathbf{S} \rangle / n_h$ and $n_h = 5$ is the number of holes. We see that both quantities decrease as the dimerization increases. This is a clear indication of the weakened coupling between the orbital and the spin for stronger dimerization strengths.

The value of $\langle \mathbf{L} \cdot \mathbf{S} \rangle$ decreases from 2 to 1. An expectation value of 2 is significantly larger than expected for a single hole in the $j_{\rm eff} = \frac{1}{2}$. Additionally, we want to understand the decrease in the expectation value for increasing V. Let us first consider the limit $10Dq \gg \zeta$, which allows us to focus on the change in the spin-orbit coupling. When increasing the value of V, the levels split [Fig. 3(a)]. The limiting values of the spin-orbit coupling of the different states for $V \to \infty$ are $\langle \mathbf{l} \cdot \mathbf{s} \rangle = \frac{1}{2}, 0, -\frac{1}{2}$ which are all two-fold degenerate. This can be understood by viewing the t_{2g} orbitals as the effective p orbitals from Eq. (1). The dimerization takes the real xy orbital

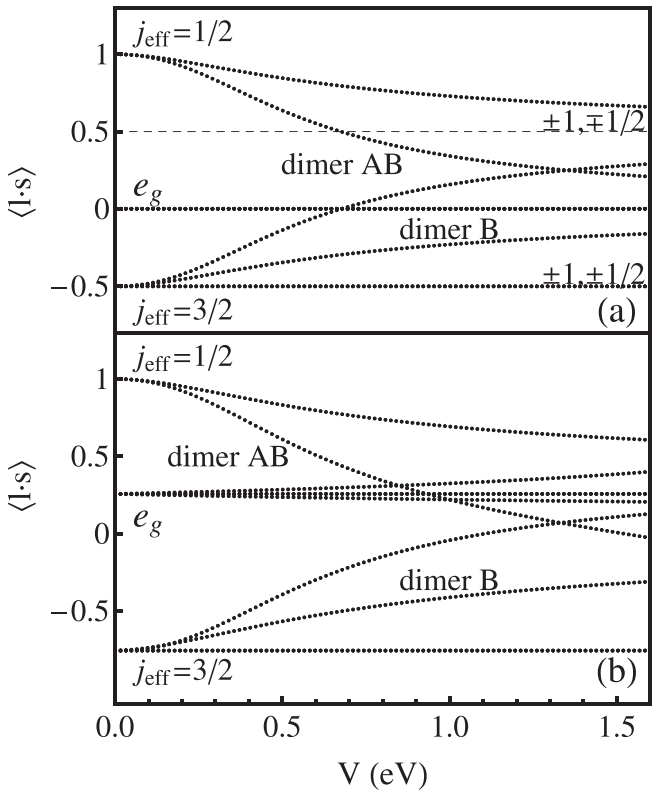

FIG. 3. (a) The expectation value $\langle \mathbf{l}\cdot\mathbf{s}\rangle$ of the different states as a function of the hopping matrix element V in the limit $10Dq \gg \zeta$. The $j_{\rm eff}$ refers to $V = 0$, whereas the label $m_{\rm eff}, \sigma$ with $m_{\rm eff} = \pm 1$ and $\sigma = \pm\frac{1}{2}$ refer to the $V \gg \zeta$ limit. (b) The same for $10Dq = 3.2$ eV.

and makes it part of the dimer. The xy is the equivalent to the $m_{\rm eff} = 0$ component of the effective p orbital. Since the dimer states are now removed in energy from the $m_{\rm eff} = \pm 1$ components, the off-diagonal terms L_-S_+ and L_+S_- in the spin-orbit interaction are suppressed. This prevents the formation of the $j_{\rm eff}$ states, see Eq. (2). Therefore, the only part of the spin-orbit interaction that remains is the diagonal component L_zS_z. This reduces the expectation value to $\langle \mathbf{l}\cdot\mathbf{s}\rangle = -m_{\rm eff}\sigma = -\frac{1}{2}, 0, \frac{1}{2}$ for $m_{\rm eff}\sigma = \pm 1, \pm\frac{1}{2}; 0, \pm\frac{1}{2}; \pm 1, \mp\frac{1}{2}$. This explains the limiting values in Fig. 3(a). Note that the decrease is relatively slow and the asymptotic values are not yet reached for the maximum V values in the plot. In the very large V limit, the dimers are composed of the orbitals with $\langle \mathbf{l}\cdot\mathbf{s}\rangle = 0$. The other states still have a spin-orbit coupling of $\pm\frac{1}{2}$. However, since both states are occupied, this does not lead to a finite ground-state expectation value of the spin-orbit coupling.

The situation becomes somewhat more complex when the e_g orbitals are included, see Fig. 3(b). For $V = 0$, the $j_{\rm eff} = \frac{1}{2}$ has $\langle \mathbf{l}\cdot\mathbf{s}\rangle = 1$, which is the same as in the limit $10Dq \gg \zeta$. However, the fourfold-degenerate $j_{\rm eff} = \frac{3}{2}$ and the e_g states have the same irreducible representation and are therefore coupled via the spin-orbit interaction. This causes a shift in the values of $\langle \mathbf{l}\cdot\mathbf{s}\rangle$, see Fig. 3(b). For $V = 0$, the shift for e_g states is of the order of $3\zeta/10Dq \cong 0.28$, which is close to the numerical value [22,23]. The total expectation value is therefore the sum of the spin-orbit coupling of the four empty e_g and the $j_{\rm eff} = \frac{1}{2}$ orbital. The numerical value is $\langle \mathbf{L}\cdot\mathbf{S}\rangle = 2.02$ giving $r = 0.41$. The resulting branching ratio is 4.04, see Figs. 2(b) and 2(c).

Upon increasing V and the resulting dimerization, the trends of the expectation values are comparable to the limit $10Dq \gg \zeta$, although the actual values are shifted somewhat. The values of $\langle \mathbf{l}\cdot\mathbf{s}\rangle$ for the e_g orbitals are relatively unchanged, so they do not affect the total spin-orbit coupling too much. The decrease in $\langle \mathbf{L}\cdot\mathbf{S}\rangle$ is primarily due to the partial quenching of the orbital moment of the t_{2g}-derived orbitals when the dimer is formed. For $V = 1.3$ eV, $\langle \mathbf{L}\cdot\mathbf{S}\rangle = 1.19$ and the branching ratio has dropped to 2.9, see Figs. 2(b) and 2(c). This change in branching ratio explains the trend in the x-ray absorption spectra, see Fig. 1, and agrees with the experiment [2,3]. The L_2 increases in intensity due to the decrease in the spin-orbit coupling as $j_{\rm eff}$ states are destroyed by the increasing dimerization. Note that the t_{2g} intensity is zero in the $V = 0$ limit. There is a slight shift of the L_2 towards lower energy due to the increased excitations into the antibonding dimer. For the L_3 edge, we already noted that the feature at 11.22 keV becomes less pronounced due to the decreased energy splitting with the e_g states [see Fig. 2(a)]. Additionally, the reduced spin-orbit coupling causes a reduction in intensity of the excitations into the t_{2g} states at the L_3 edge.

Here we used an independent-particle picture to study the dimerization. The presence of an on-site Coulomb repulsion U between electrons reduces the effects of dimerization. This can be seen by the following argument. Occupying the bonding states of Eq. (5) gives a state

$$|B\uparrow; B\downarrow\rangle = \frac{\cos\theta}{\sqrt{2}}(|xy_1\uparrow\, xy_2\downarrow\rangle + |xy_1\downarrow\, xy_2\uparrow\rangle) + \frac{\sin\theta}{\sqrt{2}}(|xy_1\uparrow\, xy_1\downarrow\rangle + |xy_2\downarrow\, xy_2\uparrow\rangle),$$

with $\tan 2\theta = 4V/U$. The energy of this state is $E_- = \frac{1}{2}(U - \sqrt{U^2 + 16V^2})$. In the limit $V \gg U$, $\theta \to \frac{\pi}{4}$ and each of the configurations in the state above becomes equally likely giving an energy for the two-electron eigenstate of $-2V + U/2$. In the limit $U \gg V$, the energy is $-4V^2/U$. This is more like an effective exchange mechanism between spins on neighboring sites. Here, U and V are comparable in magnitude. For ground-state properties, U effectively reduces the effects of dimerization.

The Coulomb repulsion also plays a role in the excitation spectra. For XAS, the effects are relatively small since an electron is put into the antibonding states. Since the bonding states are full, the electron always feels U leading to an effective shift in the XAS spectra. This situation changes for resonant inelastic x-ray scattering (RIXS) [19]. The lowest particle-conserving excitation states for the dimer are to the nonbonding states at $E = 0$, U giving excitation energies of $-E_-$ and $U - E_-$, respectively. The development of the RIXS spectra is in agreement with the calculation in this paper. At ambient pressure, only local transitions between the $j_{\rm eff} = \frac{1}{2}$ and $\frac{3}{2}$ states are observed. At high pressure, this feature collapses and increased intensity at 1.4–1.9 eV and 2.6–3.3 eV is observed. From *ab initio* calculations [19], we know that there is a sizable bonding-antibonding splitting of 2.4 eV giving $V \cong 1.2$ eV. For $V = 1.1$–1.3 eV and $U = 1.5$ eV [16,28],

excitations to the nonbonding states at 0 and U are expected at energies 1.6–2.0 eV and 3.1–3.5 eV, respectively.

III. CONCLUSION

In this paper, the effects of dimerization on the local j_{eff} states are studied. The general trend is that dimerization reduces the spin-orbit coupling in the lowest unoccupied states. This is because the dimerization involves one of the real t_{2g} orbitals whose orbital moment is quenched. When the dimerization strength V is very strong, the antibonding state of the dimer, see Eq. (5), is unoccupied. In the large V limit, only the t_{2g} orbital that partakes in the dimerization, say the xy orbital, is half filled and the orbital moment is quenched. The other t_{2g} orbitals, yz and zx, are affected by the spin-orbit interaction and form atomic-like orbitals with $m = \pm 1$. However, since both are occupied this does not contribute to the ground-state expectation value of the spin-orbit coupling. For a more realistic value of V, a small spin-orbit coupling from the t_{2g} can still occur due to the coupling of the antibonding xy state and the $m = \pm 1$ orbitals. The size of this contribution depends strongly on the energy splitting between them. Additional contributions to $\langle \mathbf{L} \cdot \mathbf{S} \rangle$ come from the e_g orbitals. The results are obtained for a system where both iridium atoms in the dimer are tetravalent (d^5-d^5). Similar conclusions were obtained for dimers of mixed valence d^4-d^5 [29] where a reduction of magnetism was found. It is worth noting that dimer formation results in a strong suppression of local magnetic moment (both spin and orbital degrees of freedom) regardless of whether the dimers are described with an independent particle wave function or with a two-electron wave function. The pressure-induced dimerization observed in β-Li_2IrO_3 [2,6] is accompanied not only by the suppression of magnetic order, but also by suppression of local Ir magnetic moments as seen both in the reduction of the high-temperature paramagnetic susceptibility and effective paramagnetic moment [3,7].

The shifts in energy and the quenching of the orbital moment with increased strength of dimerization agree with previously published XAS work [2,3]. The increase in bonding-antibonding splitting with pressure is clearly observed in the L_3 edge, where the pre-edge arising from transitions into empty antibonding states shifts closer to the absorption peak corresponding to excitations into the empty e_g states. The branching ratio, directly related to the ground-state expectation value of the spin-orbit coupling $\langle \mathbf{L} \cdot \mathbf{S} \rangle$, is strongly reduced at high strength of dimerization. Since the bonding states are delocalized over both atoms in the dimer, the direction of the moments on iridium are no longer fixed. This destroys the long-range magnetic order and the local moments. The good agreement between the theoretical model and experimental results provides clear confirmation of the competition between the formation of molecular orbitals and j_{eff} states in compressed β-Li_2IrO_3.

ACKNOWLEDGMENTS

Work at Argonne National Laboratory was supported by the U. S. DOE, Office of Science, Office of Basic Energy Sciences, under Contract No. DE-AC02-06CH11357.

[1] A. Kitaev, Ann. Phys. (NY) **321**, 2 (2006).
[2] L. S. I. Veiga, K. Glazyrin, G. Fabbris, C. D. Dashwood, J. G. Vale, H. Park, M. Etter, T. Irifune, S. Pascarelli, D. F. McMorrow, T. Takayama, H. Takagi, and D. Haskel, Phys. Rev. B **100**, 064104 (2019).
[3] L. S. I. Veiga, M. Etter, K. Glazyrin, F. Sun, C. A. Escanhoela, G. Fabbris, J. R. L. Mardegan, P. S. Malavi, Y. Deng, P. P. Stavropoulos, H. Y. Kee, W. G. Yang, M. van Veenendaal, J. S. Schilling, T. Takayama, H. Takagi, and D. Haskel, Phys. Rev. B **96**, 140402(R) (2017).
[4] V. Hermann, M. Altmeyer, J. Ebad-Allah, F. Freund, A. Jesche, A. A. Tsirlin, M. Hanfland, P. Gegenwart, I. I. Mazin, D. I. Khomskii, R. Valenti, and C. A. Kuntscher, Phys. Rev. B **97**, 020104(R) (2018).
[5] J. P. Clancy, H. Gretarsson, J. Sears, Y. Singh, S. Desgreniers, K. Mehlawat, S. Layek, G. K. Rozenberg, Y. Ding, M. Upton *et al.*, npj Quantum Mater. **35**, 1 (2018).
[6] T. Takayama, A. Krajewska, A. S. Gibbs, A. N. Yaresko, H. Ishii, H. Yamaoka, K. Ishii, N. Hiraoka, N. P. Funnell, C. Bull, and H. Takagi, Phys. Rev. B **99**, 125127 (2019).
[7] B. Shen, A. Jesche, M. Seidler, F. Freund, P. Gegenwart, and A. Tsirlin, Phys. Rev. B **104**, 134426 (2021).
[8] N. P. Breznay, A. Ruiz, A. Frano, W. Bi, R. J. Birgeneau, D. Haskel, and J. G. Analytis, Phys. Rev. B **96**, 020402(R) (2017).
[9] G. Fabbris, A. Thorn, W. Bi, M. Abramchuk, F. Bahrami, J. H. Kim, T. Shinmei, T. Irifune, F. Tafti, A. N. Kolmogorov, and D. Haskel, Phys. Rev. B **104**, 014102 (2021).
[10] G. Jackeli and G. Khaliullin, Phys. Rev. Lett. **102**, 017205 (2009).
[11] K. Modic, T. E. Smidt, I. Kimchi, N. Breznay, A. Biffin, S. Choi, R. Johnson, R. Coldea, P. Eatkins-Curry, G. McCandless, J. Y. Chan, F. Gandara, Z. Islam, A. Vishwanath, A. Shekhter, R. D. McDonald, and J. G. Analytis, Nat. Commun. **5**, 4203 (2014).
[12] X. Liu, T. Berlijn, W.-G. Yin, W. Ku, A. Tsvelik, Y.-J. Kim, H. Gretarsson, Y. Singh, P. Gegenwart, and J. P. Hill, Phys. Rev. B **83**, 220403(R) (2011).
[13] S. C. Williams, R. D. Johnson, F. Freund, S. Choi, A. Jesche, I. Kimchi, S. Manni, A. Bombardi, P. Manuel, P. Gegenwart, and R. Coldea, Phys. Rev. B **93**, 195158 (2016).
[14] A. Biffin, R. D. Johnson, S. Choi, F. Freund, S. Manni, A. Bombardi, P. Manuel, P. Gegenwawrt, and R. Coldea, Phys. Rev. B **90**, 205116 (2014).
[15] A. Biffin, R. Johnson, I. Kimchi, R. Morris, A. Bombardi, J. Analytis, A. Vishwanath, and R. Coldea, Phys. Rev. Lett. **113**, 197201 (2014).
[16] H.-S. Kim, E. Kin-Ho Lee, and Y. Baek Kim, Europhys. Lett. **112**, 67004 (2015).
[17] J. Chaloupka, G. Jackeli, and G. Khaliullin, Phys. Rev. Lett. **110**, 097204 (2013).
[18] E. Kin-Ho Lee and Y. B. Baek Kim, Phys. Rev. B **91**, 064407 (2015).
[19] T. Takayama, A. Kato, R. Dinnebier, J. Nuss, H. Kono, L. S. I. Veiga, G. Fabbris, D. Haskel, and H. Takagi, Phys. Rev. Lett. **114**, 077202 (2015).

[20] M. Majumder, R. S. Manna, G. Simutis, J. C. Orain, T. Dey, F. Freund, A. Jesche, R. Khasanov, P. K. Biswas, E. Bykova, N. Dubrovinskaia, L. S. Dubrovinsky, R. Yadav, L. Hozoi, S. Nishimoto, A. A. Tsirlin, and P. Gegenwart, Phys. Rev. Lett. **120**, 237202 (2018).

[21] P. Fulde, *Electron Correlations in Molecules and Solids* (Springer, Berlin, 1991).

[22] M. A. Laguna-Marco, D. Haskel, N. Souza-Neto, J. C. Lang, V. V. Krishnamurthy, S. Chikara, G. Cao, and M. van Veenendaal, Phys. Rev. Lett. **105**, 216407 (2010).

[23] D. Haskel, G. Fabbris, M. Zhernenkov, P. P. Kong, C. Q. Jin, G. Cao, and M. van Veenendaal, Phys. Rev. Lett. **109**, 027204 (2012).

[24] J. S. Griffith, *The Theory of Transition-Metal Ions* (Cambridge University Press, Cambridge, England, 1961).

[25] B. J. Kim, H. Jin, S. J. Moon, J.-Y. Kim, B.-G. Park, C. S. Leem, J. Yu, T. W. Noh, C. Kim, S.-J. Oh, J. H. Park, V. Durairaj, G. Cao, and E. Rotenberg, Phys. Rev. Lett. **101**, 076402 (2008).

[26] J. C. Slater and G. F. Koster, Phys. Rev. **94**, 1498 (1954).

[27] G. van der Laan and B. T. Thole, Phys. Rev. Lett. **60**, 1977 (1988).

[28] Y. Yamaji, Y. Nomura, M. Kurita, R. Arita, and M. Imada, Phys. Rev. Lett. **113**, 107201 (2014).

[29] S. V. Streltsov and D. I. Khomskii, Proc. Natl. Acad. Sci. **113**, 10491 (2016).